IN-66
205038
9P

NASA Technical Memorandum 106497

Controllability of Free-Piston Stirling Engine/ Linear Alternator Driving a Dynamic Load

M. David Kankam
National Aeronautics and Space Administration
Lewis Research Center
Cleveland, Ohio

and

Jeffrey S. Rauch
Sverdrup Technology, Inc.
Lewis Research Center Group
Brook Park, Ohio 44142

Prepared for the
28th Intersociety Energy Conversion Engineering Conference
cosponsored by ANS, SAE, ACS, IEEE, ASME, AIAA, and AIChE
Atlanta, Georgia, August 8–13, 1993

NASA

Controllability of Free-Piston Stirling Engine/Linear Alternator Driving a Dynamic Load

M. David Kankam
National Aeronautics and Space Administration
Lewis Research Center
Cleveland, Ohio 44135

Jeffrey S. Rauch
Sverdrup Technology, Inc.
Lewis Research Center Group
Brook Park, Ohio 44142

Abstract

This paper presents the dynamic behavior of a Free-Piston Stirling Engine/linear alternator (FPSE/LA) driving a single-phase fractional horse-power induction motor. The controllability and dynamic stability of the system are discussed by means of sensitivity effects of variations in system parameters, engine controller, operating conditions and mechanical loading on the induction motor. The approach used expands on a combined mechanical and thermodynamic formulation employed in a previous paper [Ref. 7]. The application of state-space technique and frequency domain analysis enhances understanding of the dynamic interactions.

Engine-alternator parametric sensitivity studies, similar to those of the previous paper, are summarized. Detailed discussions are provided for parametric variations which relate to the engine controller and system operating conditions. The results suggest that the controllability of a FPSE-based power system is enhanced by proper operating conditions and built-in controls.

Introduction

The potential for long life and reliability has culminated in the consideration of the Free-Piston Stirling Engine/linear alternator (FPSE/LA) for space power applications. This realization has generated widespread interest in the modelling and analysis of the FPSE, for better understanding of its performance characteristics. Earlier papers [Refs. 1 to 6] have dealt mainly with the FPSE and its dynamics, with minimal treatment of, or no reference to the electrical portion of the subsystem, namely, the LA. Some of the more recent papers [Refs. 7,8] have included a more detailed analysis of the LA. The results in Reference [7], on a FPSE/LA connected to a resistive load, provide useful information on the engine-alternator-load interactions, and may be used to guide system design and/or experimental efforts. In the potential application of the FPSE/LA in space power systems, there is a high probability that there will be more dynamic than static loads. The introduction of a dynamic load into any existing power source-load interactions complicates the system sufficiently to warrant an assessment of the resulting system behavior.

This paper describes the control and dynamic stability analysis of an FPSE/LA feeding into a single-phase, fractional horse-power induction motor which is driving a comparably-sized fan load. The engine/LA is the Space Power Research Engine, SPRE, [Ref. 9] at the NASA Lewis Research Center, which was used in Reference [7]. The analysis is based on a combination of dynamic and thermodynamic analysis of the Stirling engine [Refs. 7, 10], circuit theory of the electrical system and state-space technique in modern control theory [Ref. 11]. Dynamic stability is determined from computation of eigenvalues of the linearized system matrix, using the MATLAB software [Ref. 12]. Controllability of the integrated system is evaluated by parametric sensitivities on the eigenvalues, to show the potential of a FPSE/LA-dynamic load application in space power system.

System Representation

Figure 1 depicts the equivalent circuit of the system of study. It comprises a Free-Piston Stirling Engine coupled with a linear alternator (FPSE/LA), connected via control circuitry to a single-phase induction motor. A connected fan is driven by the induction motor-generated electromagnetic torque. The parameter C_T is a tuning capacitor for optimum power transfer to the motor-fan load. The term R_P denotes a parasitic load for controlling the system through maintenance of power balance between the generation source and the motor-fan load. The resistor R_c is inserted to determine its effectiveness in controlling the system during load-side fault.

The parameters r_S and L_{1S} represent the induction motor stator winding resistance and leakage inductance, respectively, of the motor. The magnetizing branch of the air-gap is denoted by L_m. The parameters L_{1r} and r_r are the rotor leakage inductance and winding resistance, respectively, referred to the stator side. The rotor slip, S, is a measure of how much the frequency of the rotor-induced field lags the stator field.

Equations of the system dynamic behavior are derived, based on Fig. 1 and the schematic representation of the FPSE in Fig. 2.

Development of System Equations

The key FPSE equations are summarized. The equations of the electrical portion of the system are developed next. The mechanical-thermodynamic and electrical equations together are then cast in a state-space notation. Dynamic stability analysis is then performed.

Summary of FPSE Equations

The dynamic equations of the FPSE relate to the single cylinder representation in Fig. 2, and are based on the assumptions below:

(1) Schmidt's thermodynamic analysis is evoked such that:

(a) the displacer and piston motions and the working space pressure are sinusoidal.

(b) the working fluid obeys the ideal gas law, and expands and compresses isothermally.

(2) The working space gas pressure is spatially constant but time-variant.

(3) The bounce space pressure balances the average working space pressure. Hence, average positions of the power piston, displacer and cylinder casing are stationary.

The detailed development of the pertinent equations is described in Reference [7]. The engine mechanical and thermodynamic properties are included. The resulting dynamic equations are stated in Eqn. (1), where the definitions of the terms are summarized in Table 1.

$$\begin{bmatrix} m_D & 0 \\ 0 & m_P \end{bmatrix}\begin{bmatrix} \ddot{X}_D \\ \ddot{X}_P \end{bmatrix} = -\begin{bmatrix} C_{11} & C_{12} \\ C_{21} & C_{22} \end{bmatrix}\begin{bmatrix} \dot{X}_D \\ \dot{X}_P \end{bmatrix} - \begin{bmatrix} K_{11} & K_{12} \\ K_{21} & K_{22} \end{bmatrix}\begin{bmatrix} X_D \\ X_P \end{bmatrix} + \begin{bmatrix} 0 \\ F_{EP} \end{bmatrix} \quad (1)$$

where

$$\begin{bmatrix} C_{11} & C_{12} \\ C_{21} & C_{22} \end{bmatrix} = \begin{bmatrix} (C_{DD}+C_{T11}) & (C_{DP}+C_{T12}) \\ (C_{PD}+C_{T21}) & (C_{PP}+C_{T22}) \end{bmatrix}$$

$$\begin{bmatrix} K_{11} & K_{12} \\ K_{21} & K_{22} \end{bmatrix} = \begin{bmatrix} (K_{DD}+K_{T11}) & (K_{DP}+K_{T12}) \\ (K_{PD}+K_{T21}) & (K_{PP}+K_{T22}) \end{bmatrix}$$

$$[C_T] = \begin{bmatrix} C_{T11} & C_{T12} \\ C_{T21} & C_{T22} \end{bmatrix} = \begin{bmatrix} -A_D \dfrac{\partial P_{HX}}{\partial \dot{X}_D} & -A_D \dfrac{\partial P_{HX}}{\partial \dot{X}_P} \\ 0 & 0 \end{bmatrix}$$

$$[K_T] = \begin{bmatrix} K_{T11} & K_{T12} \\ K_{T21} & K_{T22} \end{bmatrix} = \begin{bmatrix} A_R \dfrac{\partial P_c}{\partial X_D} & A_R \dfrac{\partial P_c}{\partial X_P} \\ A_P \dfrac{\partial P_c}{\partial X_D} & A_P \dfrac{\partial P_c}{\partial X_P} \end{bmatrix}$$

Equations of LA-Dynamic Load Subsystem

The loop equations of loops 1 through 4 in Fig. 1. are summarized in Eqns. (2) through (6), respectively, using Kirchhoff's voltage law. The notation $\dot{f}$ represents $\frac{df}{dt}$.

$$(R_a + R_p + R_c)\, i_g + (L_a + L_{ma})\, \dot{i}_g - R_p i_L + V_{C_T} = e_g \equiv -\left(N \frac{d\Phi}{dX_p}\right)\dot{X}_p \quad (2)$$

$$-R_p i_g + (r_s + R_p)\, i_L + (L_{ls} + L_m)\, \dot{i}_L - 0.5L_m \dot{i}_f - 0.5L_m \dot{i}_b = 0 \quad (3)$$

$$-0.5L_m \dot{i}_L + 0.5 \frac{r_r'}{S} i_f + 0.5(L_m + L_{lr}')\, \dot{i}_f = 0 \quad (4)$$

$$-0.5L_m \dot{i}_L + 0.5 \frac{r_r'}{(2-S)} i_b + 0.5(L_m + L_{lr}')\, \dot{i}_b = 0 \quad (5)$$

$$\dot{V}_{C_T} = i_g / C_T \quad (6)$$

The term $\left(N\frac{d\Phi}{dX_p}\right)\dot{X}_p$ is the voltage generated by the piston-induced flux change. The loop currents i_f and i_b relate to the forward and backward rotating fields in the rotor [Ref. 13]. The electrodynamic differential equation (7) relates to the dynamics of the induction machine-fan load. The

$$Jw_r = T_e - kw_r^2 \quad (7)$$

parameters J and w_r are the respective inertia and rotational velocity of the induction machine rotor, k is the rotational constant of proportionality for the fan. The nominal value of k is chosen to correspond to the 0.33 hp rating of the induction motor. The terms R_f and R_b are the resistive components of the impedances Z_f and Z_b of the forward and backward rotating circuits in Fig. 1. The derivation of the electromagnetic torque T_e, developed by the induction machine yields Eqn. (8), where w_{ex} is the excitation angular velocity of the stator

$$T_e = CONST2 * i_L^2 = ((1-S)\,(R_f - R_b)\, P_p/4w_{ex})\, i_L^2 \quad (8)$$

winding. The slip S of the forward field relates to the relative motion of flux and rotor conductors, with subsequent induced rotor voltage of slip frequency Sf_{ex}. The parameter P_p is the number of poles on the induction machine.

System Dynamic Stability

The combined dynamic equations of the FPSE and the circuit and electrodynamic equations of the electrical-mechanical load subsystems may be linearized for dynamic stability analysis. State variable representation [Ref. 11] of the linearized equations enable easy computation of the system eigenvalues.

State-Space Formulation

The nonlinearities in Eqns. (7) and (8) are removed by linearization about the steady-state operation. Neglect of second order incremental terms results in Eqn. (9).

$$J\Delta w_r = (2.CONST2.i_{L_O})\,\Delta i_L - 2\,kw_{ro}\,\Delta w_r \qquad (9)$$

The system state variable vector in terms of incremental changes may be defined as in the transposed (T) Eqn. (10).

$$[X]^T \equiv [X_1\ X_2\ X_3\ X_4\ X_5\ X_6\ X_7\ X_8\ X_9\ X_{10}]$$

$$= [\Delta X_D\ \Delta X_D\ \Delta X_p\ \Delta X_p\ \Delta i_g\ \Delta V_{cT}\ \Delta i_L\ \Delta i_f\ \Delta i_b\ \Delta w_r] \qquad (10)$$

Substitution of Eqn. (10) into Eqns. (1) through (6) and (9) results in the state-space equation (11), where

$$[X] = [A][X] \qquad (11)$$

the system [A] matrix is defined in Eqn. (12). The matrix entries in relation to the system parameters are summarized in Table 2.

Discussions of the dynamic stability analysis on the eigenvalues of the [A] matrix follow.

Results of Sensitivity Analysis

Simulation of the system behavior under varying parameters and operating conditions is performed, using the MATLAB software [Ref. 12]. The results of the simulation appear in Figs. 3 through 10. The base or reference system results of Fig. 3 are obtained from the use of the nominal parameters in Table 1. The FPSE and LA subsystems are the same as those used in Reference [7], namely, the SPRE engine [Ref. 9]. Subsequent figures show the particular parameter being varied, while the remaining parameters are kept at the nominal values. The physical meaning of the eigenvalue location in the complex plane is given by the modal response, such as illustrated in Fig. 4 of Reference [7].

Fig. 3 shows the electrical, piston and displacer roots E1, MP and MD, respectively, of the coupled, and the corresponding roots E1U, MPU and MDU of the uncoupled FPSE and LA plus associated control parameters C_T and R_P. Similarly to the presentation in Reference [7], these roots yield the same information with regard to the design (105 Hz) and operating (101.1 Hz) frequencies, respectively, of the SPRE engine. Also, Redlich and Berchowitz's observation [Ref. 4] of the piston root, MPU, in the right-hand plane is confirmed. This root is indicative of an oscillator with amplitudes which tend towards its mechanical limits. Furthermore, the coupled system's reduction in the margin of operating-point stability of the electrical subsystem is evident.

The presence of the induction machine load yields additional three electrical roots E2, E3 and E4. These roots are associated with the main field of the stator, and the backward and forward rotating fields of the rotor, respectively. The real-only nature of these roots signifies that, for the small horse-power (1/3 hp) machine in question, any inherent electric transients are typically highly damped. In Fig. 1, the portion to the right of the R_p branch is the steady-state equivalent circuit of the single-phase induction motor. The absence of machine transients from the circuit eliminates any conjugate complex eigenvalues which may otherwise be present for the machine. The real negative roots are consistent with the normal operating mode of the induction motor, illustrated in the torque-speed (T-w), curve of Fig. 4. Generally, the motor operates on the negative slope portion of the curve, at the intersection point of its mechanical load and the T-w curves. The negativity of the E2, E3 and E4 roots denotes a stable operation in the negative slope region, following a small disturbance about the operating point.

Figure 3 forms the basis of comparison with the parametric variations, described next.

Parametric Variations

The effect on dynamic stability, due to 50 to 150 percent of nominal value variations in LA resistance Ra, is minimal, while that of La is moderate. This finding is similar to that reported in Reference [7]. The impact of 0 to 150 percent change in the control resistor, Rc, is found to be similar to that of Ra. This is evident from Fig. 5, and consistent with the circuit topology of Fig. 1.

Effect of tuning capacitance (CT) - Root locus migration caused by 50 to 150 percent change in nominal CT is shown in Fig. 6. Here and elsewhere in the sensitivity results, the nominal eigenvalue is arrowed, where necessary. The trend is similar to that discussed in Reference [7]. The impact on the piston (MP), displacer (MD) and LA circuit (E1) roots is significant. However, the induction motor roots E2, E3 and E4 remain stationary, due to their highly damped nature. Evidently, nominal value of CT yields a near optimum placement of the MP root on the jw-axis.

Effect of parasitic load (Rp) - The variation in Rp is likened to an automatic controller in a practical system. However, such incremental changes from 25 to 200 percent of the nominal value do not account for the

nonlinearities inherent in a physical controller. Nonetheless, the trends portrayed by Rp in Fig.7 illustrate the potential effectiveness of a properly designed controller in maintaining system stability.

Other than the roots of the induction motor main and backward rotating fields, all remaining roots are appreciably affected by the parasitic load. The decay of the LA circuit root, E1, and the induction motor root, E4, becomes more damped, as Rp increases in value. The optimum Rp is the nominal value beyond which the displacer root MD loses some margin of stability, and the piston root MP crosses the jw-axis to become dynamically unstable. At the optimum Rp, by virtue of the piston root on the jw-axis and all others in the left-half plane (LHP), the FPSE/LA subsystem behaves as an oscillator.

Effect of stator short circuit - Typically, system short circuit is not a planned event. However, it can happen inadvertently. Figure 8 shows the impact of such an event on the system stability. Compared to Fig. 3, it is evident that the short circuit forces the induction motor roots onto the origin. Also, the stability margins of the FPSE/LA roots are reduced, as the roots move closer towards the right half plane (RHP). The dominance of the control resistor R_{c1} in the remaining circuit following the short circuit, assures a near oscillator and stable mode of operation. The value of R_{c1} should be chosen to ensure system stability at fault condition, while minimizing the dissipative loss, due to R_{c1}, during normal operation of the power system.

During the fault condition, the parasitic load Rp is effectively shorted and, as such, has no effect on the system roots behavior.

Effect of slip (S) - Variations in motor slip are directly related to changes in the induction motor rotor speed. A higher slip implies a lower rotor speed, and vice versa. An operating induction motor will slow down, if its mechanical load, such as a fan, is increased. The net result will be a higher slip value. The converse is true. The operating slip is determined by the point of intersection of the torque-speed and the mechanical load curves, namely, point A or B in Fig. 4.

Figure 9 depicts the system root migration due to increasing the motor slip from 25 to 300 percent of the nominal value (0.05). Slip has negligible effect on the dynamics of the FPSE/LA subsystem. This is partly attributable to the relatively small size induction motor-fan load (less than 1kWe), compared to the 12kWe FPSE/LA subsystem. Also, Fig. 9 shows that the motor stator main field root, E2, is independent of slip. The effect on the rotor forward field root, E4, is relatively more pronounced than that on the backward field root, E3. Higher slips reduce the stability margin of E4, and slightly increase that of E3. These observations can be verified from examining the forward and backward field circuit impedances, Zf and Zb, respectively, in Fig. 1.

Effect of no load operation - An excited induction motor without mechanical load will run at a slip value based on the design requirements of the motor. Fig. 10 shows the system roots at sudden disconnection of the fan load from the motor. Comparison with Fig. 3 of the base system shows that the rotor backward field root, E3, collapses onto the origin, thereby losing its dynamics. However, all the remaining roots remain virtually unaffected. Thus, for the relatively small induction motor/fan load, loss of the mechanical load is not expected to substantially affect the dynamic stability of the rest of the system.

Conclusions

This paper describes the control and dynamic stability of FPSE/LA-induction motor/fan system. The analysis applies modern control theory to a combined dynamic model of the FPSE/LA and circuit and electrodynamic model of the motor/fan load to compute eigenvalues of the system. The controllability of the system is assessed from the effects of parametric variations on the eigenvalues. The key results are summarized below.

A system fault, such as a load-side short circuit, can potentially force the roots of the dynamic load on to the origin and reduce stability margin for the FPSE/LA subsystem. The presence of a control resistor on the FPSE/LA circuit side promotes a desired oscillatory behavior of the engine. A sudden increase in the mechanical load beyond the rating of the induction motor can reduce the stability of the motor. Depending on the relative sizes of the FPSE/LA and the connected load, loss of the mechanical load during steady-state operation may not substantially affect the system performance.

The overall results indicate that, with proper design and operating conditions and controls, a power system comprising a FPSE/LA driving a dynamic load can remain dynamically stable.

References

1. Rauch, J. S., *"Steady-state Analysis of Free-Piston Stirling Engine Dynamics,"* IECEC '75 Record, pp. 961-965.
2. Das, R. L. Bahrami, K. A., *"Dynamics and Control of Stirling Engines in a 15 kWe Solar Electric*

Generation Concept," Proce. IECEC 1979, pp. 133-138.

3. Cichy, M. Carlini, M., *"Frequency Dynamic Analysis of Free-Piston Stirling Engines,"* IECEC 1984, pp. 1829-1835.
4. Redlich, R. N., Berchowitz, D. M., *"Linear Dynamics of Free-Piston Stirling Engines,"* Proc. Instr. Mech. Engrs., Vol. 199, #A3, pp. 203-213, 1985.
5. Carlini, M. Kucharski, T., *"Dynamic Analysis of Free-Piston Stirling Engines by Modal Transformation Method,"* Presented at SAE Intl. Congress and Exposition, Detroit, MI, Feb. 24-28, 1986.
6. Benvenuto, G., DeMonte, F., Farina, F., *"Dynamic Behavior Prediction of Free-Piston Stirling Engines,"* IECEC 1990, pp. 346-351.
7. Kankam, M. D., Rauch, J. S., *"Dynamic Analysis of Free-Piston Stirling Engine/Linear Alternator-Load system - Experimentally Validated,"* 27th IECEC, August 1992, San Diego.
8. Fu, Z. X., Nasar, S. A., *"Stability Analysis of a Free-Piston Stirling Engine Power Generation System,"* 27th IECEC, August 1992, San Diego.
9. *"Space Power Demonstrator Engine,"* Phase I Final Report, NASA Contractor Report 179555, May 1987.
10. Kankam, M. D., Rauch, J. S., *"Comparative Survey of Dynamic Analyses of Free-Piston Stirling Engines,"* IECEC, August 1991, Boston.
11. *"Modern Control Theory,"* Book, by W. L. Brogan, Prentice-Hall., 1982.
12. *"MAC II MATLAB,"* Copyright The Mathwork, 1987, 1988.
13. Fitzgerald, A. E., Kingsley Jr., C., Umans, S. D., *"Electric Machinery,"* Book 5th Ed., McGraw-Hill, 1990.

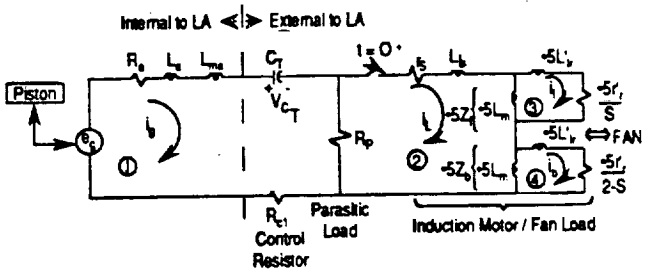

Fig. 1. Equivalent Circuit of Linear Alternator (LA) -Dynamic Load System

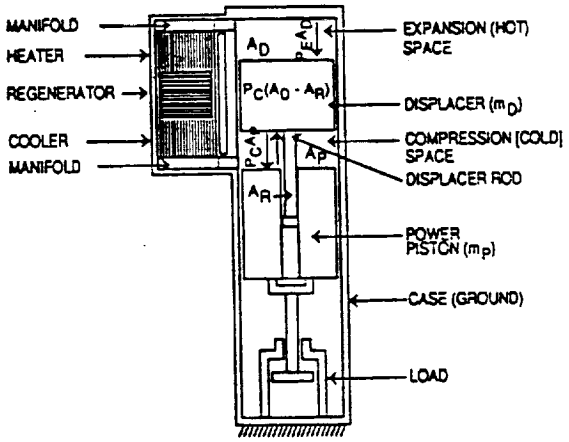

Fig. 2 Schematic of a Single Cylinder Free-Piston Stirling Engine

$$[A] = \begin{bmatrix} -K_{11}/m_D & 1/C_{11}/m_D & -K_{12}/m_D & -C_{12}/m_D & & & & & & \\ & & & 1 & & & & & & \\ -K_{21}/m_P & -C_{12}/m_P & -K_{22}/m_P & -C_{22}/m_P & NF/m_P & & & & & \\ & & & -NFTP_3 & -P1 & -P3 & P2 & & & \\ & & & & 1/C_T & & & & & \\ & & & & P4 & & -P5 & -P6 & -P7 & \\ & & & & P8 & & -P9 & P12 & -P13 & \\ & & & & P8 & & -P9 & -P10 & P11 & \\ & & & & & & \frac{2*CONST2*i_{LO}}{J} & & & \frac{-2\,kW_{rO}}{J} \end{bmatrix} \quad (12)$$

Note: BLANK ENTRIES ARE ZEROS

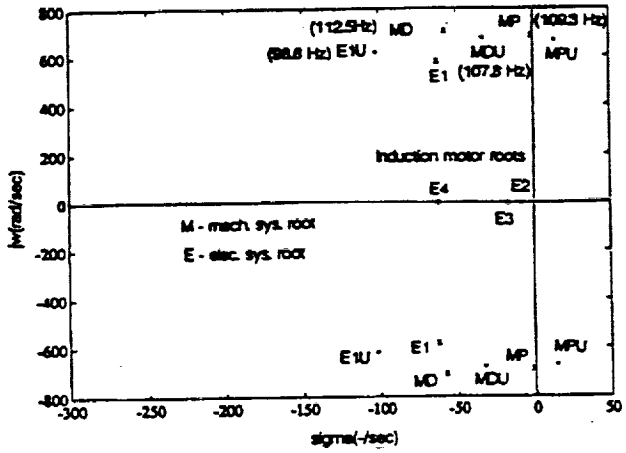

Fig. 3 Coupled and decoupled system eigenvalues

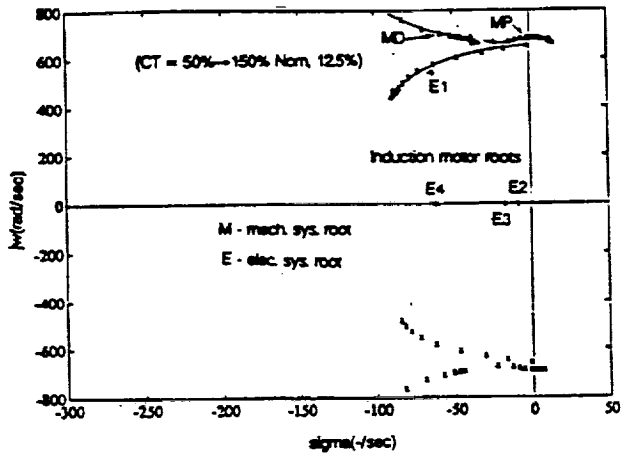

Fig. 6 System eigenvalues with CT variation

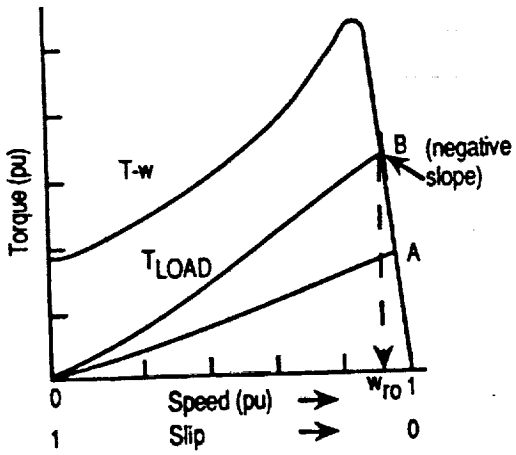

Fig. 4 Induction motor torque-speed curve and curves of load torque.

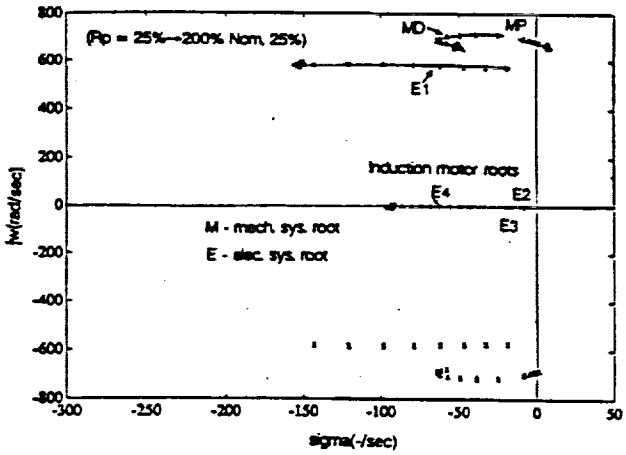

Fig. 7 System eigenvalues with Rp variation

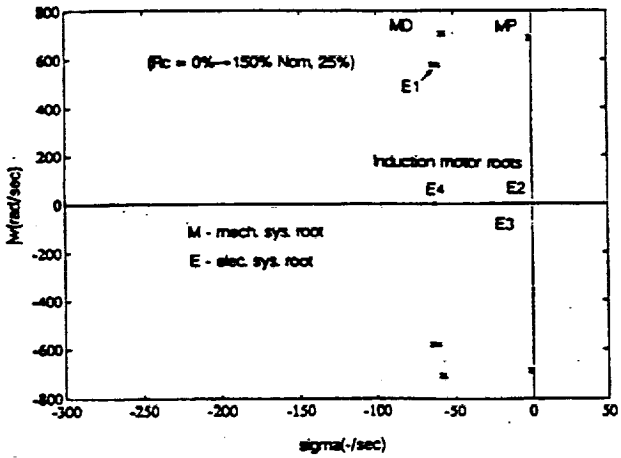

Fig. 5 System eigenvalues with Rc variation

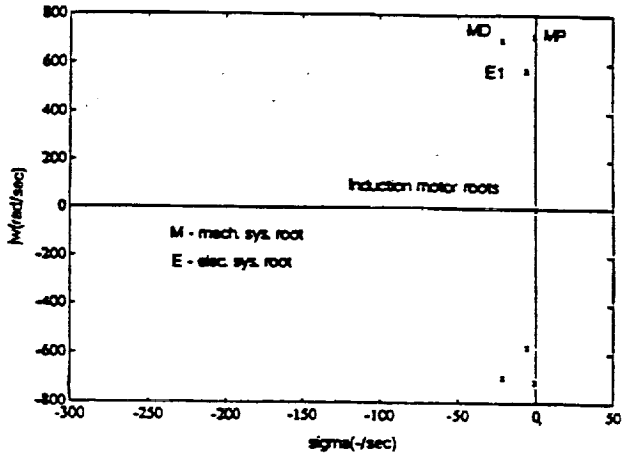

Fig. 8 System eigenvalues with stator short circuit

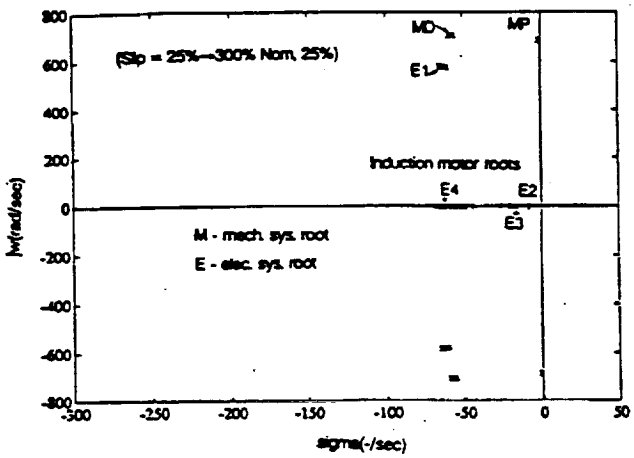

Fig. 9 System eigenvalues with slip variation

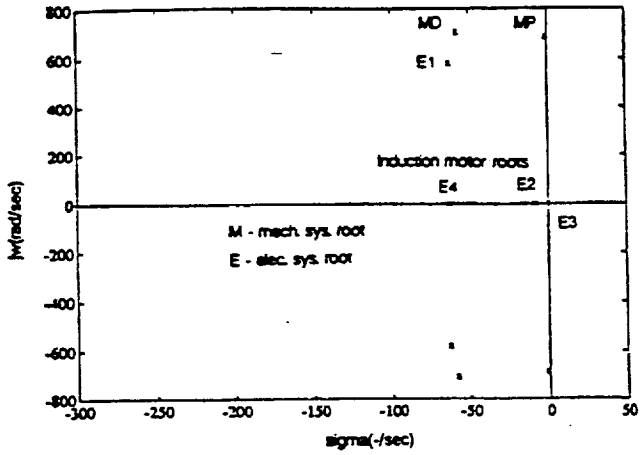

Fig. 10 System eigenvalues without mechanical load

Table 1. Summary of System Parameters (Nominal Values Shown)

Subsystem	Symbol	Value	Description
FP Stirling Engine	m_d	1.701 (kg)	Displacer mass
	m_p	9.968 (kg)	Piston mass
	A_p	164.63 x 10^{-4} (m^2)	Piston area
	A_d	102.61 x 10^{-4} (m^2)	Displacer area
	A_r	2.887 x 10^{-4} (m^2)	Piston rod area
	K_{dd}	8.1197 x 10^5 (N/m)	Displacer total stiffness coefficient
	C_{dd}	54.95 (N.S/m)	Displacer total damping coefficient
	K_{pp}	12.205 x 10^5 (N/m)	Piston total stiffness coefficient
	C_{pp}	60.85 (N.S/m)	Piston total damping coefficient
	K_{pd}	0 (N/m)	Displacer-piston coupling stiffness coefficient
	K_{dp}	0 (N/m)	Piston-displacer coupling stiffness coefficient
	C_{pd}	0 (N.S/m)	Displacer-piston coupling damping coefficient
	C_{dp}	0 (N.S/m)	Piston-displacer coupling damping coefficient
	$\frac{\partial P_C}{\partial X_p}$	186.562 x 10^6 (N/m^3)	Compression space pressure change with piston position
	$\frac{\partial P_C}{\partial X_d}$	-24.98 x 10^6 (N/m^3)	Compression space pressure change with displacer position
	$\frac{\partial P_C}{\partial \dot{X}_p}$	0 ($N.S/m^3$)	Compression space pressure change with piston velocity
	$\frac{\partial P_C}{\partial \dot{X}_d}$	0 ($N.S/m^3$)	Compression space pressure change with displacer velocity
	$\frac{\partial P_{HX}}{\partial X_p}$	0 (N/m^3)	Heat exchanger pressure change with piston position
	$\frac{\partial P_{HX}}{\partial X_d}$	0 (N/m^3)	Heat exchanger pressure change with displacer position
	$\frac{\partial P_{HX}}{\partial \dot{X}_d}$	0 ($N.S/m^3$)	Heat exchanger pressure change with displacer velocity
	$\frac{\partial P_{HX}}{\partial \dot{X}_p}$	0 ($N.S/m^3$)	Heat exchanger pressure change with piston velocity
	$N\frac{d\phi}{dx_p}$	45.5 (V-S/m)	Magnetic flux linkage change with piston position
Linear Alternator	R_a	0.082 (Ω)	LA winding resistance
	L_a	1.95 (mH)	LA leakage inductance
	L_{ma}	6.50 (mH)	LA magnetizing inductance
	C_T	296.3 (μF)	Tuning capacitance
	R_p	1.6655 (Ω)	Parasitic Load
	R_c	0.082 (Ω)	Control Resistor
Single-Phase Induction Motor	r_s	1.59 (Ω)	Stator main winding resistance
	L_{ls}	5.2 (mH)	Stator main winding leakage inductance
	L_m	89.9 (mH)	Magnetizing inductance
	L'_{lr}	6.9 (mH)	Rotor leakage inductance (referred to stator)
	r'_r	1.869 (Ω)	Rotor resistance (referred to stator)
	S	0.05	Operating slip

Table 2 Definition of Matrix [A] Entries (Ref: Fig. 1.)

Parameter	Definition
DENOM	$L_{ls} + L_m L'_{lr}/(L_m + L'_{lr})$
TNUM	$L_m/(L_m + L'_{lr})$
SUM	$L_m (0.5 L_m + L'_{lr}) + L_{ls}(L_m + L'_{lr})$
P1	$L_{ls} + L_m L'_{lr}/(L_m + L'_{lr})$
P2	$R_p/(L_a + L_{ma})$
P3	$1/(L_a + L_{ma})$
P4	R_p/DENOM
P5	$(r_s + R_p)$/DENOM
P6	r'_r*TNUM/(2*S*DENOM)
P7	S*P6/(2-S)
P8	TNUM*P4
P9	TNUM*P5
P10	TNUM*P6
P11	$-r'_r$*SUM/((2-S) $(L_m + L'_{lr})^2$*DENOM)
P12	(2-S) *P11/S
P13	S*P10 / (2-S)

REPORT DOCUMENTATION PAGE

Form Approved
OMB No. 0704-0188

1. AGENCY USE ONLY (*Leave blank*)	2. REPORT DATE	3. REPORT TYPE AND DATES COVERED
	February 1994	Technical Memorandum

4. TITLE AND SUBTITLE
Controllability of Free-Piston Stirling Engine/Linear Alternator Driving a Dynamic Load

5. FUNDING NUMBERS
WU–590–13–11

6. AUTHOR(S)
M. David Kankam and Jeffrey S. Rauch

7. PERFORMING ORGANIZATION NAME(S) AND ADDRESS(ES)
National Aeronautics and Space Administration
Lewis Research Center
Cleveland, Ohio 44135–3191

8. PERFORMING ORGANIZATION REPORT NUMBER
E–8488

9. SPONSORING/MONITORING AGENCY NAME(S) AND ADDRESS(ES)
National Aeronautics and Space Administration
Washington, D.C. 20546–0001

10. SPONSORING/MONITORING AGENCY REPORT NUMBER
NASA TM–106497

11. SUPPLEMENTARY NOTES
Prepared for the 28th Intersociety Energy Conversion Engineering Conference cosponsored by ANS, SAE, ACS, IEEE, ASME, AIAA, and AIChE, Atlanta, Georgia, August 8–13, 1993. M. David Kankam, NASA Lewis Research Center and Jeffrey S. Rauch, Sverdrup Technology, Inc., Lewis Research Center Group, 2001 Aerospace Parkway, Brook Park, Ohio 44142 (work funded by NASA Contract NAS3–25266). Responsible person, M. David Kankam, organization code 5430, (216) 433–6143.

12a. DISTRIBUTION/AVAILABILITY STATEMENT
Unclassified - Unlimited
Subject Category 66

12b. DISTRIBUTION CODE

13. ABSTRACT (*Maximum 200 words*)

This paper presents the dynamic behavior of a Free-Piston Stirling Engine/linear alternator (FPSE/LA) driving a single-phase fractional horse-power induction motor. The controllability and dynamic stability of the system are discussed by means of sensitivity effects of variations in system parameters, engine controller, operating conditions and mechanical loading on the induction motor. The approach used expands on a combined mechanical and thermodynamic formulation employed in a previous paper [Ref. 7]. The application of state-space technique and frequency domain analysis enhances understanding of the dynamic interactions. Engine-alternator parametric sensitivity studies, similar to those of the previous paper, are summarized. Detailed discussions are provided for parametric variations which relate to the engine controller and system operating conditions. The results suggest that the controllability of a FPSE-based power system is enhanced by proper operating conditions and built-in controls.

14. SUBJECT TERMS	15. NUMBER OF PAGES
Free-piston Stirling engine; Dynamic load; Dynamic stability; Controllability; State-space technique	9
	16. PRICE CODE: A02

17. SECURITY CLASSIFICATION OF REPORT	18. SECURITY CLASSIFICATION OF THIS PAGE	19. SECURITY CLASSIFICATION OF ABSTRACT	20. LIMITATION OF ABSTRACT
Unclassified	Unclassified	Unclassified	